J. Earth Syst. Sci. (2020)129 2
https://doi.org/10.1007/s12040-019-1268-5

Tangential winds of a vortex system in a planetary surface layer

Shefali Uttam[1,2], Deepak Singh[1] and Varun Sheel[1,*]

[1]*Physical Research Laboratory, Ahmedabad, India.*
[2]*Indian Institute of Technology, Gandhinagar, India.*
**Corresponding author. e-mail: varun@prl.res.in*

MS received 27 March 2019; revised 12 July 2019; accepted 18 July 2019

The planetary boundary layer (PBL) mediates interactions between the surface and free atmosphere. In Martian PBL, surface can force convective vortices leading to dust devils. We use the Navier–Stokes equations and the continuity equation to determine mean (with respect to time) tangential wind velocity in cylindrical co-ordinate system within the surface layer of a planetary atmosphere. We utilize Martian surface layer properties for theoretical derivation of our solution. However, our results remain valid for any planetary surface layer as long as all of our assumptions are valid. Our theoretical values of the tangential wind velocity lie well within the range of observed values. The derived equation represents the dependency of tangential velocity on both radial distances from the center of vortex, and the altitude. As we move further away from the vortex center, the effect of vortex becomes non-significant, and velocities start following the standard logarithmic profile. Due to dependency of tangential wind velocity on altitude, the tangential velocity increases as we move higher up in the vortex system. At 100 m altitude, for an order of magnitude increase in the radial distance, the mean tangential wind velocity drops by about a factor of 1.5 in magnitude.

Keywords. Atmosphere dynamics; Mars atmosphere; planetary dynamics; terrestrial planets.

1. Introduction

The circulation of wind in the atmosphere is driven by the pressure gradient developed between two locations, incoming energy from the Sun, and the rotation of the planet. The Navier–Stokes (NS) equations describe the motion of viscous fluid substances and are a formulation of the conservation of momentum of the system. NS equations or momentum equations in inertial frame of reference can be given as (Schlichting *et al.* 1955):

$$\frac{Du_i}{Dt} = -\frac{1}{\rho}\frac{\partial p}{\partial x_i} + \nu\frac{\partial^2 u_i}{\partial x_j^2} - g\,\delta_{i3}, \tag{1}$$

where u_i is the component of fluid velocity, ρ is the density of the fluid, ν is the kinematic viscosity of the fluid (= dynamic viscosity (μ)/density of fluid (ρ)), p is the pressure in the surrounding, and g is the acceleration due to gravity of the planet.

The Navier–Stokes equations in rotational frame of reference (tensorial notation) for incompressible fluid, are given as (Schlichting *et al.* 1955; Dong and Wu 2015):

$$\frac{\partial u_i}{\partial t} + v_j\frac{\partial u_i}{\partial x_j} = -\frac{1}{\rho}\frac{\partial p}{\partial x_i} + \nu\frac{\partial^2 u_i}{\partial x_j^2} - g\,\delta_{i3} - 2\,\Omega\,\epsilon_{ijk}\,\eta_j\,u_k, \tag{2}$$

where Ω is the angular rotation of the planet. Though the Navier–Stokes equations represent

Published online: 19 December 2019

winds in any part of an atmosphere, modeling the wind profiles in the boundary layer is challenging (Petrosyan *et al.* 2011; Bryan *et al.* 2017). A two dimensional set of Navier–Stokes equations reduces from an elliptical equation to a parabolic equation in the boundary layer under certain assumptions which is easier to solve (Davis *et al.* 1986; Bell *et al.* 1989). Here, we will follow a different approach to find wind profile in a boundary layer.

On Mars, the atmospheric boundary layer extends up to an altitude of about 10 km as compared to about 1 km on Earth (Petrosyan *et al.* 2011). The Earth's daytime surface layer extends up to about 0.1 km. However, the Mars' daytime surface layer can extend up to 1 km (Petrosyan *et al.* 2011). The logarithmic layer (figure 1c) gets its name due to the fact that the vertical profile of wind velocity is approximately logarithmic in this particular layer. The expression for the mean horizontal wind velocity (for logarithmic layer) in Cartesian co-ordinate system is given as (Zheng 2009):

$$\bar{u} = \frac{u_*}{k} ln \frac{z}{z_0}, \tag{3}$$

where, u_* is the threshold friction velocity near surface, 'k' is von Karman constant, z is the altitude, and z_0 is the aerodynamic roughness length of the surface. The roughness parameter measures the effectiveness of a surface structure to absorb momentum and is the height where the extrapolated wind flow approaches zero or at which the turbulent fluid flow become laminar. The above semi-empirical relationship describes the vertical distribution of horizontal mean wind speeds within the lowest 1 km of the planetary boundary layer. The logarithmic variation of horizontal wind velocity is not valid in mixing layer or above due to high fluctuations in physical parameters like pressure, temperature, and density with altitude.

A cylindrical co-ordinate system is a three-dimensional coordinate system that specifies point positions by the distance from a chosen reference axis, the direction from the axis relative to a chosen reference direction, and the distance from a chosen reference plane perpendicular to the axis (Moon and Spencer 2012). The expression for mean horizontal velocity of wind in the Cartesian co-ordinate system provides a good approximation for atmospheric wind movement in the logarithmic layer of any planet. However, this expression fails to accurately determine the tangential velocity of wind for a vortex system such as dust devil, tornado, and storms.

Significant amount of dust loading occurs during dust storms in Martian atmosphere. However, the mechanism of dust lifting is still debatable. One mechanism could be, for example, vortical eruptions resulting from instabilities induced by a convective vortex which could lead to concentrated vortices or dust devils (Sengupta *et al.* 2003, 2018). Events like dust-devils, occur very frequently in the Martian climate system (Ryan and Lucich 1983; Metzger *et al.* 1999; Greeley *et al.* 2006; Stanzel *et al.* 2006; Reiss *et al.* 2011). Therefore, accurate estimation of wind velocity in such climate system is very important for understanding

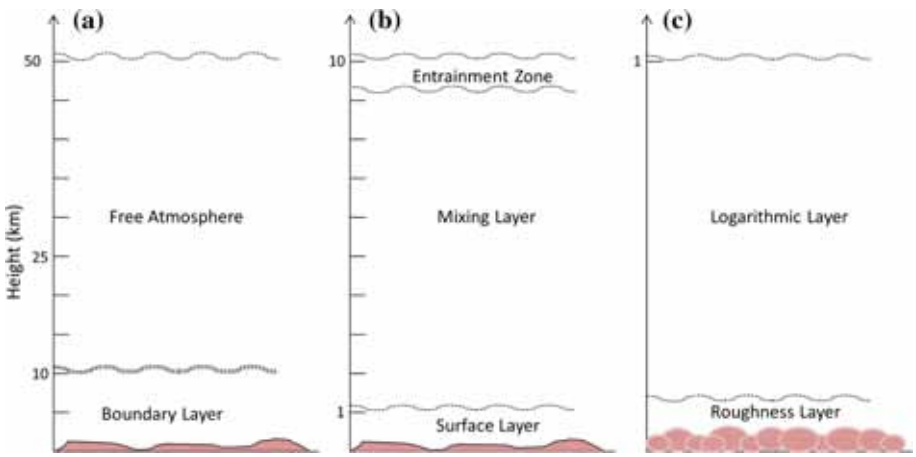

Figure 1. Typical vertical structure of Martian atmosphere. **(a)** The atmosphere is divided into two broad zones viz., daytime convective boundary layer and free atmosphere. **(b)** The boundary layer can be further divided into surface layer, mixing layer and entrainment zone. **(c)** The surface layer consists of a roughness layer and a logarithmic layer.

that system's behaviour. Most often, a cylindrical system is used for experiments or simulations of vortex systems (e.g., Williamson 1996; Huang *et al.* 2008; Horton *et al.* 2016). Therefore, we consider a cylindrical vortex system to estimate the wind velocity variation with radial distance from vortex center, and altitude. In this paper, we derive the equation of mean tangential velocity of wind in cylindrical co-ordinate system (for planetary surface layer) using NS and continuity equations. Our co-ordinate system coincides with the center of vortex system at surface. We assume our vortex system to be in steady-state. In a steady-state condition, the structure of a vortex system does not undergo any change with time. The velocity field around the vortex is always normal to both the symmetry axis 'z' and the radial vector 'r'. We do not consider any effect of translational motion of the vortex in estimation of our velocity. We also compare our results with observed tangential velocities of vortex on Earth for validation of our results.

2. Tangential winds for a vortex derived from NS equations in a cylindrical co-ordinate system

Figure 2 shows a schematic of cylindrical vortex system with mean tangential wind flowing in anti-clockwise direction. The continuity equation for an incompressible flow of fluid (tensorial notation) is given as:

$$\frac{\partial u_i}{\partial x_i} = 0. \tag{4}$$

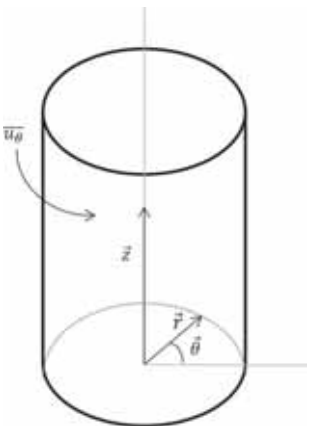

Figure 2. Cylindrical vortex system with mean tangential wind ($\overline{u}_\theta$).

In the cylindrical coordinate system, the equations of atmospheric flow are expressed with components (u, u_θ, u_z) of velocity vector $\vec{u}$. Therefore, the continuity equation can be expressed as:

$$\frac{\partial u_r}{\partial r} + \frac{u_r}{r} + \frac{1}{r}\frac{\partial u_\theta}{\partial \theta} + \frac{\partial u_z}{\partial z} = 0. \tag{5}$$

According to atmospheric boundary layer theory, the Coriolis force near the surface layer can be neglected (Zheng 2009). Again, if the horizontal scale of a disturbance is small enough, the Coriolis force may be neglected compared to the pressure gradient force, and the centrifugal force. The Rossby number (Ro), $Ro = V/f\,L$, where V is the wind-speed, $f = 2\ \Omega \sin\phi$ is the Coriolis parameter (Ω is the angular frequency of planetary rotation and ϕ is the latitude), and L is the length scale of vortex that determines the relative significance of various forces with each other. For Mars surface layer winds, $V = 10\ \mathrm{ms}^{-1}$, $L = 100$ m and $f = 10^{-4}\ \mathrm{s}^{-1}$ leads to $Ro \approx 10^3$, which implies that the Coriolis force can be neglected as compared to other forces. Moreover, atmospheric motions are usually modelled within the shallow-fluid approximation. This simplifies the three-dimensional spherical geometry, and for dynamical consistency the Coriolis force is neglected. We consider the incompressible flow of the fluid, which is an important condition for applying Boussinesq approximations. The Boussinesq approximation ignores density differences except where they appear in terms multiplied by gravity 'g'. The idea behind the Boussinesq approximation is to restrict the analysis to that of systems whose overall background density and temperature do not vary much around their mean values. The mathematical form for pressure, density and temperature using Boussinesq approximation can be given as:

$$\begin{aligned} P &= P_0(z) + p(\vec{r}), \quad \rho = \rho_0(z) + \rho'(\vec{r}), \\ T &= T_0(z) + T'(\vec{r}), \end{aligned} \tag{6}$$

where $P_0(z)$, $\rho_0(z)$, and $T_0(z)$ are the time-averaged values of pressure, density and temperature of the fluid respectively, and $p(\vec{r})$, $\rho'(\vec{r})$, $T'(\vec{r})$ are the fluctuations in this time-averaged values of pressure, density, and temperature of the fluid respectively.

The adiabatic lapse rate for atmosphere is:

$$\frac{\partial T_0}{\partial z} = -\frac{g}{C_p}. \tag{7}$$

The hydrostatic equilibrium equation is:

$$\frac{\partial P_0}{\partial z} = -g\rho_0. \tag{8}$$

Using equations (6–8), the three components of the NS equations can be written as:

(a) The r-component:

$$\frac{\partial u_r}{\partial t} + u_r\frac{\partial u_r}{\partial r} + \frac{u_\theta}{r}\frac{\partial u_r}{\partial \theta} + u_z\frac{\partial u_r}{\partial z} = -\frac{1}{\rho_0}\left(\frac{\partial p}{\partial r}\right) + \frac{u_\theta^2}{r} + \nu\left(\frac{\partial^2 u_r}{\partial r^2} + \frac{\partial^2 u_r}{\partial z^2} + \frac{1}{r^2}\frac{\partial^2 u_r}{\partial \theta^2} - \frac{2}{r^2}\frac{\partial u_\theta}{\partial \theta} + \frac{1}{r}\frac{\partial u_r}{\partial r} - \frac{u_r}{r^2}\right). \tag{9}$$

(b) The θ-component:

$$\frac{\partial u_\theta}{\partial t} + u_r\frac{\partial u_\theta}{\partial r} + \frac{u_\theta}{r}\frac{\partial u_\theta}{\partial \theta} + u_z\frac{\partial u_\theta}{\partial z} = -\frac{1}{\rho_0}\frac{1}{r}\left(\frac{\partial p}{\partial \theta}\right) - \frac{u_r u_\theta}{r} + \nu\left(\frac{\partial^2 u_\theta}{\partial r^2} + \frac{\partial^2 u_\theta}{\partial z^2} + \frac{1}{r^2}\frac{\partial^2 u_\theta}{\partial \theta^2} + \frac{2}{r^2}\frac{\partial u_r}{\partial \theta} + \frac{1}{r}\frac{\partial u_\theta}{\partial r} - \frac{u_\theta}{r^2}\right). \tag{10}$$

(c) The z-component:

$$\frac{\partial u_z}{\partial t} + u_r\frac{\partial u_z}{\partial r} + \frac{u_\theta}{r}\frac{\partial u_z}{\partial \theta} + u_z\frac{\partial u_z}{\partial z} = -\frac{1}{\rho_0}\left(\frac{\partial p}{\partial z}\right) - g\frac{\rho'}{\rho^0} + \nu\left(\frac{\partial^2 u_z}{\partial r^2} + \frac{\partial^2 u_z}{\partial z^2} + \frac{1}{r^2}\frac{\partial^2 u_z}{\partial \theta^2} + \frac{1}{r}\frac{\partial u_z}{\partial r}\right). \tag{11}$$

Applying linearity, i.e., $\frac{\rho'}{\rho_0} = \frac{-T'}{T_0}$ to equation (11), and with further simplification we get:

$$\frac{\partial u_z}{\partial t} + u_r\frac{\partial u_z}{\partial r} + \frac{u_\theta}{r}\frac{\partial u_z}{\partial \theta} + u_z\frac{\partial u_z}{\partial z} = -\frac{1}{\rho_0}\left(\frac{\partial p}{\partial z}\right) + g\frac{T'}{T_0} + \nu\left(\frac{\partial^2 u_z}{\partial r^2} + \frac{\partial^2 u_z}{\partial z^2} + \frac{1}{r^2}\frac{\partial^2 u_z}{\partial \theta^2} + \frac{1}{r}\frac{\partial u_z}{\partial r}\right). \tag{12}$$

Chain rule for some partial differential terms in equations (10–12) is as follows:

$$u_r\frac{\partial u_r}{\partial r} + \frac{u_\theta}{r}\frac{\partial u_r}{\partial \theta} + u_z\frac{\partial u_r}{\partial z} = \frac{\partial(u_r u_z)}{\partial z} + \frac{1}{r}\frac{\partial(r u_r u_r)}{\partial r} + \frac{1}{r}\frac{\partial(u_r u_\theta)}{\partial \theta}, \tag{13}$$

$$u_r\frac{\partial u_\theta}{\partial r} + \frac{u_\theta}{r}\frac{\partial u_\theta}{\partial \theta} + u_z\frac{\partial u_\theta}{\partial z} = \frac{\partial(u_\theta u_z)}{\partial z} + \frac{1}{r}\frac{\partial(r u_r u_\theta)}{\partial r} + \frac{1}{r}\frac{\partial(u_\theta u_\theta)}{\partial \theta}, \tag{14}$$

$$u_r\frac{\partial u_z}{\partial r} + \frac{u_\theta}{r}\frac{\partial u_z}{\partial \theta} + u_z\frac{\partial u_z}{\partial z} = \frac{\partial(u_z u_z)}{\partial z} + \frac{1}{r}\frac{\partial(r u_r u_z)}{\partial r} + \frac{1}{r}\frac{\partial(u_z u_\theta)}{\partial \theta}. \tag{15}$$

After applying chain rule (equations 13–15), the three components of the NS equations (equations 9–12) will be simplified to:

(a) The r-component:

$$\frac{\partial u_r}{\partial t} + \frac{1}{r}\frac{\partial(r u_r u_r)}{\partial r} + \frac{1}{r}\frac{\partial(u_r u_\theta)}{\partial \theta} + \frac{\partial(u_r u_z)}{\partial z} = -\frac{1}{\rho_0}\left(\frac{\partial p}{\partial r}\right) + \frac{u_\theta^2}{r} + \nu\left(\frac{\partial^2 u_r}{\partial r^2} + \frac{\partial^2 u_r}{\partial z^2} + \frac{1}{r^2}\frac{\partial^2 u_r}{\partial \theta^2} - \frac{2}{r^2}\frac{\partial u_\theta}{\partial \theta} + \frac{1}{r}\frac{\partial u_r}{\partial r} - \frac{u_r}{r^2}\right). \tag{16}$$

(b) The θ-component:

$$\frac{\partial u_\theta}{\partial t} + \frac{1}{r}\frac{\partial(r u_\theta u_r)}{\partial r} + \frac{1}{r}\frac{\partial(u_\theta u_\theta)}{\partial \theta} + \frac{\partial(u_\theta u_z)}{\partial z} = -\frac{1}{\rho_0}\frac{1}{r}\left(\frac{\partial p}{\partial \theta}\right) - \frac{u_r u_\theta}{r} + \nu\left(\frac{\partial^2 u_\theta}{\partial r^2} + \frac{\partial^2 u_\theta}{\partial z^2} + \frac{1}{r^2}\frac{\partial^2 u_\theta}{\partial \theta^2} + \frac{2}{r^2}\frac{\partial u_r}{\partial \theta} + \frac{1}{r}\frac{\partial u_\theta}{\partial r} - \frac{u_\theta}{r^2}\right). \tag{17}$$

(c) The z-component:

$$\frac{\partial u_z}{\partial t} + \frac{1}{r}\frac{\partial(r u_r u_z)}{\partial r} + \frac{1}{r}\frac{\partial(r u_\theta u_z)}{\partial \theta} + \frac{\partial(u_z u_z)}{\partial z} = -\frac{1}{\rho_0}\left(\frac{\partial p}{\partial z}\right) - g\frac{T'}{T_0} + \nu\left(\frac{\partial^2 u_z}{\partial r^2} + \frac{\partial^2 u_z}{\partial z^2} + \frac{1}{r^2}\frac{\partial^2 u_z}{\partial \theta^2} + \frac{1}{r}\frac{\partial u_z}{\partial r}\right). \tag{18}$$

According to the Reynolds-averaged treatment (Reynolds 1895; Adrian *et al.* 2000), an instantaneous quantity is decomposed into its time-averaged and fluctuating quantities, i.e., $\vec{u}(\vec{r},t) = \overrightarrow{\bar{u}}(\vec{r},t) + \vec{u}'(\vec{r},t)$. This treatment is primarily used to describe turbulent flows. Using Reynolds treatment, the continuity equation (equation 5) can be re-written as:

$$\frac{1}{r}\frac{\partial(r\bar{u}_r)}{\partial r} + \frac{1}{r}\frac{\partial \bar{u}_\theta}{\partial \theta} + \frac{\partial \bar{u}_z}{\partial z} = 0. \tag{19}$$

An approximation to the Reynolds number can be given as $R_e \approx VL/\nu$ (Shao 2008), where V and L are typical velocity scale and typical length scale for a flow, respectively. The Reynolds number is the ratio of inertial forces to viscous forces and measures how turbulent the flow is. Low Reynolds number flows are laminar, while higher Reynolds number flows are turbulent. For Mars surface layer winds, $V \approx 10\ \mathrm{m\ s^{-1}}$, $L \approx 100\ \mathrm{m}$, and $\nu \approx 10^{-3}\ \mathrm{m^2\ s^{-1}}$ (Petrosyan *et al.* 2011), it follows that $R_e \approx 10^6$. The large Reynolds number indicates that the wind flows in Martian surface layers are almost always turbulent. Therefore, neglecting viscous terms in equations (16–18) (since we are dealing with turbulent region of the atmosphere); three components of Reynolds-averaged NS equations will be reduced to:

$$\begin{aligned}&\frac{\partial \bar{u}_r}{\partial t}+\bar{u}_r\frac{\partial \bar{u}_r}{\partial r}+\frac{\bar{u}_\theta}{r}\frac{\partial \bar{u}_r}{\partial \theta}+\bar{u}_z\frac{\partial \bar{u}_r}{\partial z}\\&\quad=-\frac{1}{\rho_0}\frac{\partial \bar{p}}{\partial r}-\frac{\partial\left(\overline{u_r'u_z'}\right)}{\partial z}-\frac{\partial\left(\overline{u_r'u_r'}\right)}{\partial r}-\frac{1}{r}\frac{\partial\left(\overline{u_r'u_\theta'}\right)}{\partial \theta}\\&\qquad-\frac{1}{r}\overline{u_r'u_r'}+\frac{1}{r}\overline{u_\theta u_\theta}+\frac{1}{r}\overline{u_\theta'u_\theta'},\end{aligned}\tag{20}$$

$$\begin{aligned}&\frac{\partial \bar{u}_\theta}{\partial t}+\bar{u}_r\frac{\partial \bar{u}_\theta}{\partial r}+\frac{\bar{u}_\theta}{r}\frac{\partial \bar{u}_\theta}{\partial \theta}+\bar{u}_z\frac{\partial \bar{u}_\theta}{\partial z}\\&\quad=-\frac{1}{\rho_0}\frac{\partial \bar{p}}{\partial \theta}-\frac{\partial\left(\overline{u_\theta'u_z'}\right)}{\partial z}-\frac{\partial\left(\overline{u_\theta'u_r'}\right)}{\partial r}-\frac{1}{r}\frac{\partial\left(\overline{u_\theta'u_\theta'}\right)}{\partial \theta}\\&\qquad-\frac{1}{r}\overline{u_r'u_\theta'}-\frac{1}{r}\overline{u_r u_\theta}-\frac{1}{r}\overline{u_r'u_\theta'},\end{aligned}\tag{21}$$

$$\begin{aligned}&\frac{\partial \bar{u}_z}{\partial t}+\bar{u}_r\frac{\partial \bar{u}_z}{\partial r}+\frac{\bar{u}_\theta}{r}\frac{\partial \bar{u}_z}{\partial \theta}+\bar{u}_z\frac{\partial \bar{u}_z}{\partial z}\\&\quad=-\frac{1}{\rho_0}\frac{\partial \bar{p}}{\partial z}-\frac{\partial\left(\overline{u_z'u_z'}\right)}{\partial z}-\frac{\partial\left(\overline{u_r'u_z'}\right)}{\partial r}-\frac{1}{r}\frac{\partial\left(\overline{u_z'u_\theta'}\right)}{\partial \theta}\\&\qquad-\frac{1}{r}\overline{u_r'u_z'}.\end{aligned}\tag{22}$$

The azimuthal velocity (tangential velocity) determines the rotational velocity of a rotating vortex, and amount of dust it can lift. Since we have considered the velocity field to be normal to both 'z' axis and 'r' axis, the velocity field is parallel to the θ-unit vector direction. Therefore, the net velocity field would be, $\vec{u} = u_\theta \hat{e}_\theta$. Now, we are interested in determining the variation of azimuthal velocity with height and size of the vortex. Therefore, we consider that θ-component is in the direction of mean horizontal velocity, z is in the direction of mean vertical velocity, and the ground is homogeneous with even roughness. Since Coriolis force has been already neglected, that will lead to the cyclostrophic balance in an atmospheric vortex, which satisfies:

$$\frac{V^2}{r} \approx -\frac{1}{\rho}\frac{\partial p}{\partial n},\tag{23}$$

where, n is normal to the direction of flow. After applying cyclostrophic balance, equation (21) can be simplified to:

$$\frac{\partial \bar{u}_\theta}{\partial t} = -\frac{1}{\rho_0}\frac{\partial \bar{p}}{\partial \theta}-\frac{\partial\left(\overline{u_\theta'u_z'}\right)}{\partial z}-\frac{2}{r}\overline{u_r'u_\theta'}.\tag{24}$$

Since we have taken a cylindrical symmetry, we do not expect any change in pressure in the azimuthal direction. Hence, equation (24) simplifies to:

$$\frac{\partial \bar{u}_\theta}{\partial t} = \frac{1}{\rho_0}\frac{\partial\left(-\rho_0\overline{u_\theta'u_z'}\right)}{\partial z}-\frac{2}{r}\overline{u_r'u_\theta'}.\tag{25}$$

In steady-state scenario, equation (25) can be written as:

$$\frac{1}{\rho_0}\frac{\partial\left(-\rho_0\overline{u_\theta'u_z'}\right)}{\partial z}-\frac{2}{r}\overline{u_r'u_\theta'} = \frac{1}{\rho_0}\frac{\partial \tau_{z\theta}}{\partial z}+\frac{2\tau_{r\theta}}{r\rho_0}=0,\tag{26}$$

where $\tau_{z\theta}$ and $\tau_{r\theta}$ are the components of Reynolds shear stress (Shao 2008; Stull 2012).

Reynolds shear stress ($\tau_{r\theta}$) is described using the expression $-\rho\overline{u_r'u_\theta'}$. Reynolds stress only exists when the fluid is in turbulent motion. The Reynolds shear stress deals with turbulent momentum flux which acts like a stress. The momentum flux is transferred to other layers by the fluctuating winds. Hence, the Reynolds stress becomes directly dependent on the velocity of wind, and not on the position of vortex. Since $\tau_{r\theta}$ is only a function of velocities, and not co-ordinates; we integrate equation (26) (integration limit, $z_0 \to z$) and get,

$$\tau_{z\theta} = -\frac{2(z-z_0)}{r}\tau_{r\theta}.\tag{27}$$

Turbulence shear stress can be given as (Stull 2012):

$$\tau = \sqrt{\tau_{r\theta}^2+\tau_{z\theta}^2} = \tau_{r\theta}\sqrt{1+\frac{4(z-z_0)^2}{r^2}}.\tag{28}$$

Prandtl postulated that the velocity scale of a fluctuation motion is equal to the velocity gradient

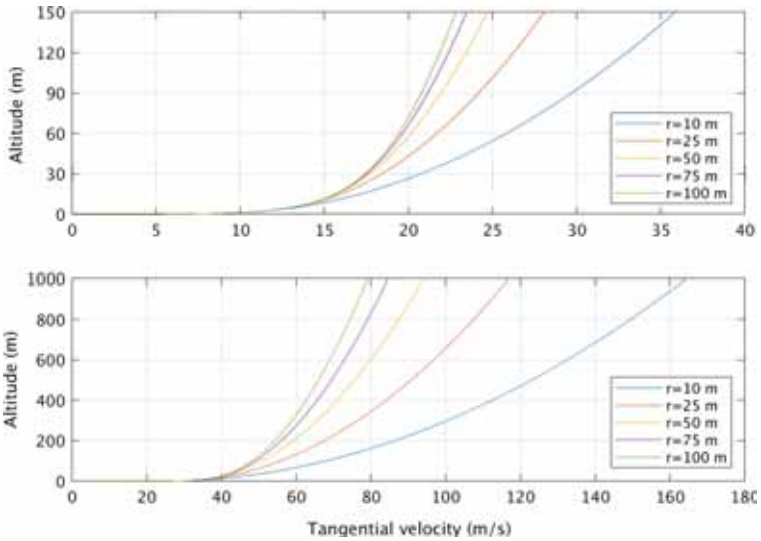

Figure 3. Comparison of tangential wind velocity profiles of Earth (top) and Mars (bottom) for various radial distances from vortex center.

times the mixing length scale (Bradshaw 1974). According to Prandtl's mixing length theory (Zheng 2009), the shear stress can be given by $\tau = \mu_t \frac{\partial \overline{u_\theta}}{\partial z}$; where $\mu_t = \rho_0 \, l_m^2 \left|\frac{\partial \overline{u_\theta}}{\partial z}\right|$, and $l_m = kz$ is mixing length. Using Prandtl's theory and equation (28), we get:

$$\tau_{r\theta}\left(1+\frac{4(z-z_0)^2}{r^2}\right)^{1/2} = \rho_0 k^2 z^2 \left|\frac{\partial \overline{u_\theta}}{\partial z}\right|^2. \qquad (29)$$

Using the expression of threshold friction $u_*\left(=\sqrt{\tau_{r\theta}/\rho_0}\right)$ velocity near surface (Shao 2008), and further simplifying equation (29):

$$\frac{\partial \overline{u_\theta}}{\partial z} = \frac{u_*}{kz}\left(1+\frac{4(z-z_0)^2}{r^2}\right)^{1/4}, \quad z \geq z_0, \qquad (30)$$

where 'r' is the distance from the center of vortex, and 'z' is the altitude from surface. Equation (30) is the analytical solution (with certain assumptions) of Navier–Stokes equations for estimating the tangential velocity for a vortex system in a planetary surface layer.

3. Results and discussions

We use trapezoidal method for numerical integration (integration limit, $z_0 \to z$) of equation (30) to determine tangential wind velocities in Earth's and Mars' surface layers. We assume values of 2 ms^{-1}, 0.4, and 0.01 m for near surface threshold friction velocity, von Karman constant, and aerodynamic roughness length of the surface respectively for a typical Martian surface layer (Sutton *et al.* 1978; Högström 1985; Newman *et al.* 2002; Petrosyan *et al.* 2011). For Earth, we assume values of 1 ms^{-1} and 0.03 m for near surface threshold friction velocity, and aerodynamic roughness length of the surface respectively (Balme *et al.* 2003; Jarraud 2008). Typical Mars' and Earth's surface layers extend up to 1000 and 150 m, respectively.

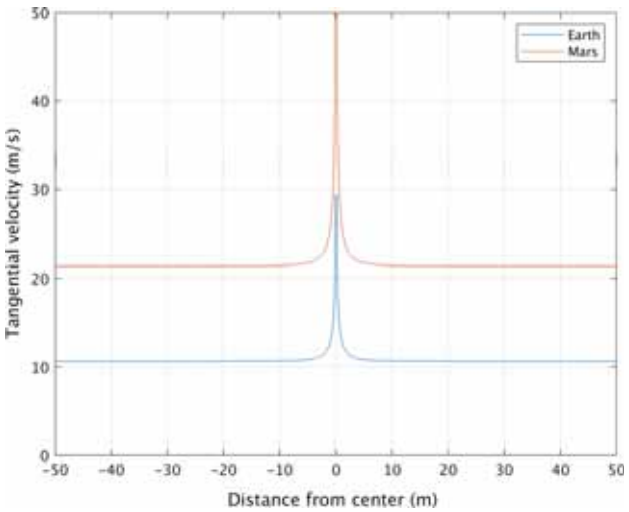

Figure 4. Comparison of tangential wind velocities on Mars and Earth due to a vortex with respect to the radial distance from center (0 being the center). Velocities are estimated at 7 ft (5.18 m) altitude from the surface.

Figure 3 shows the variation of mean tangential wind velocity with altitude for various radial distances. We observe a reduction by a factor of about

Table 1. *Theoretical tangential wind velocity ($\overline{u_\theta}$) determined using equation (30) with $z_0 = 0.03$ m, and $u_* = 1$ ms^{-1}. All velocities are in ms^{-1}.*

	$z = 7$ ft (2.13 m)	$z = 17$ ft (5.18 m)	$z = 31$ ft (9.45 m)
$r = 5$ m	10.88	13.78	16.38
$r = 10$ m	10.73	13.19	15.17

1.5 in mean velocities (at 150 m altitude for both planets) for one order increase (10–100 m) in the radial distance due to inverse square dependency on radial distance. The tangential velocities would be higher as we move closer to the center of the vortex, and decreases sharply with increasing distance. The variation in tangential velocities with variation in radial distance increases with increasing altitude and vice-versa.

Figure 4 shows the comparison of velocities between Earth and Mars surface layers at a fixed altitude (7 ft (5.18 m)) with respect to the radial distance from center (0 indicates the center) of vortex. The velocities on Mars are relatively higher as compared to velocities on Earth due to lower roughness length and higher threshold friction velocity. As we move far away from the center of a rotating vortex, the velocities in both planets' surface layers reach a saturation value which is the ambient wind speed. This happens because as *'r'* increases ($r \to \infty$), the second term in equation (30) becomes non-significant as compared to the first term, and eventually leads to logarithmic wind profiles without any effect of vortex.

3.1 *Comparison with observed data*

Sinclair (1966) measured three cylindrical components of the wind velocity through the base of a dust devil, at 7, 17, and 31 ft above the surface over a flat desert terrain near Tucson, Arizona. From these observations, it follows that the tangential wind velocity typically fluctuates between 10 and 15 ms^{-1} (Sinclair 1973).

For comparison, we theoretically determine the tangential wind velocity using equation (30), with roughness length (z_0) = 0.03 m (Jarraud 2008), and $u_* = 1$ ms^{-1} (Balme *et al.* 2003) at 7, 17, and 31 ft (2.13, 5.18 and 9.45 m) above the surface. We determine the velocities at 5 and 10 m from the center of the vortex. In general, our theoretical values of the tangential wind velocity (table 1) are well within the range of observed values. At higher altitude and close to vortex center, our values are slightly higher due to various assumptions (or approximations) we made during the mathematical formulation of our derived equation.

Cyclostrophic balance is always maintained within a vortex. Therefore, we can predict the pressure drop around a vortex using this balance if we have the knowledge of tangential velocity and *vice versa*. The cyclostrophic balance around a vortex is represented as:

$$\Delta p = \frac{v^2}{RT}\, p_{\text{avg}},$$

where, Δp is the pressure drop around the vortex, v is the tangential velocity of the vortex, R is the specific gas constant of the air, T is the background temperature and p_{avg} is the average pressure of the surrounding.

Sinclair (1966) measured the tangential velocity of the dust devil at three heights varying between 10 and 15 m/s and pressure drop varying between 1 and 3 hPa. Using the value of the reported $T = 320$ K and assuming the typical summertime values for the surface pressure $p_{\text{avg}} = 925$ hPa and $R = 287$ m^2 s^{-2} K^{-1}, we obtain the calculated pressure drop to vary between 1.2 and 2.7 hPa.

For Mars, with typical values of $T = 250$ K, $R = 192$ m^2 s^{-2} K^{-1}, and $p_{\text{avg}} = 700$ Pa and threshold velocity $v \approx 30$ ms^{-1} (Greeley *et al.* 2003), we obtain a pressure drop of $\Delta p \approx 13$ Pa.

4. Concluding remarks

We derived a simple differential equation for the mean tangential velocity in cylindrical co-ordinate system using NS equations (equation 30). The derived equation represents the dependency of tangential velocity on both distance from the center of cylinder, and the altitude. Equation (30) would be useful to estimate the variation of velocity with radial distance from vortex center. However, as we move further away from the vortex center, the second term in equation (30) becomes non-significant, and velocities start following the standard logarithmic profile. We note that, equation (30) is only valid in the planetary surface layer region of the atmosphere.

The dependency of tangential wind velocity on altitude indicates the increase in velocity as we move higher up in the vortex system. The tangential velocity of the wind also decreases as we move far away from the vortex center. At 100 m

altitude, for an order of magnitude increase in the radial distance, the mean tangential wind velocity drops by about a factor of 1.5 in magnitude. We theoretically estimated tangential velocities for both Earth and Mars surface layers. The velocities on Earth are relatively lower as compared to velocities on Mars due to higher roughness length and lower threshold friction velocity.

Comparison with observed data substantiates the validity and applicability of equation (30) for vortex systems in planetary surface layers. We believe that, this form of equation can prove very vital for determining the mean tangential wind velocities in a vortex system for planet like Mars (where vortex systems like dust devils occur frequently). Although we utilize Martian surface layer properties to derive most of our results, equation (30) remains valid for any planetary surface layer as long as all of our assumptions are valid.

References

Adrian R J, Christensen K T and Liu Z C 2000 Analysis and interpretation of instantaneous turbulent velocity fields; *Exp. Fluids* **29(3)** 275–290, https://doi.org/10.1007/s003489900087.

Balme M, Metzger S, Towner M, Ringrose T, Greeley R and Iversen J 2003 Friction wind speeds in dust devils: A field study; *Geophys. Res. Lett.* **30(16)**, https://doi.org/10.1029/2003GL017493.

Bell J B, Colella P and Glaz H M 1989 A second-order projection method for the incompressible Navier–Stokes equations; *J. Comput. Phys.* **85(2)** 257–283, https://doi.org/10.1016/0021-9991(89)90151-4.

Bradshaw P 1974 Possible origin of Prandt's mixing-length theory; *Nature* **249(5453)** 135, https://doi.org/10.1038/249135b0.

Bryan G H, Worsnop R P, Lundquist J K and Zhang J A 2017 A simple method for simulating wind profiles in the boundary layer of tropical cyclones; *Bound.-Layer Meteorol.* **162(3)** 475–502, https://doi.org/10.1007/s10546-016-0207-0.

Davis R T, Barnett M and Rakich J V 1986 The calculation of supersonic viscous flows using the parabolized Navier—Stokes equations; *Comput. Fluids* **14** 197–224, https://doi.org/10.1016/0045-7930(86)90021-6.

Dong S and Wu S 2015 A modified Navier–Stokes equation for incompressible fluid flow; *Proc. Eng.* **126** 169–173, https://doi.org/10.1016/j.proeng.2015.11.206.

Greeley R, Balme M R, Iversen J D, Metzger S, Mickelson R, Phoreman J and White B 2003 Martian dust devils: Laboratory simulations of particle threshold; *J. Geophys. Res. Planets* **108(E5)**, https://doi.org/10.1029/2002JE001987.

Greeley R, Whelley P L, Arvidson R E, Cabrol N A, Foley D J, Franklin B J, Geissler P G, Golombek M P, Kuzmin R O, Landis G A, Lemmon M T, Neakrase L D V, Squyres S W and Thompson S D 2006 Active dust devils in Gusev crater, Mars: Observations from the Mars exploration rover spirit; *J. Geophys. Res. Planets* **111(E12)**, https://doi.org/10.1029/2006JE002743.

Högström U 1985 Von Karman's constant in atmospheric boundary layer flow: Reevaluated; *J. Atmos. Sci.* **42(3)** 263–270, https://doi.org/10.1175/1520-0469(1985)042<0263:VKCIAB>2.0.CO;2.

Horton W, Miura H, Onishchenko O, Couedel L, Arnas C, Escarguel A, Benkadda S and Fedun V 2016 Dust devil dynamics; *J. Geophys. Res. Atmos.* **121(12)** 7197–7214, https://doi.org/10.1002/2016JD024832.

Huang N, Yue G and Zheng X 2008 Numerical simulations of a dust devil and the electric field in it; *J. Geophys. Res. Atmos.* **113(D20)**, https://doi.org/10.1029/2008JD010182.

Jarraud M 2008 *Guide to meteorological instruments and methods of observation (WMO-No. 8);* World Meteorological Organisation: Geneva, Switzerland, pp. I.5–13.

Metzger S M, Carr J R, Johnson J R, Parker T J and Lemmon M T 1999 Dust devil vortices seen by the Mars Pathfinder camera; *Geophys. Res. Lett.* **26(18)** 2781–2784, https://doi.org/10.1029/1999GL008341.

Moon P and Spencer D E 2012 *Field theory handbook including coordinate systems, differential equations and their solutions;* Springer, Chapter 3.

Newman C E, Lewis S R, Read P L and Forget F 2002 Modeling the Martian dust cycle, 1. Representations of dust transport processes; *J. Geophys. Res. Planets* **107(E12)**, https://doi.org/10.1029/2002JE001910.

Petrosyan A, Galperin B, Larsen S E, Lewis S R, Määttänen A, Read P L, Renno N, Rogberg L P H T, Savijärvi H, Siili T, Spiga A, Toigo A and Vázquez L 2011 The Martian atmospheric boundary layer; *Rev. Geophys.* **49(3)**, https://doi.org/10.1029/2010RG000351.

Reiss D, Zanetti M and Neukum G 2011 Multitemporal observations of identical active dust devils on Mars with the High Resolution Stereo Camera (HRSC) and Mars Orbiter Camera (MOC); *Icarus* **215(1)** 358–369, https://doi.org/10.1016/j.icarus.2011.06.011.

Reynolds O 1895 On the dynamical theory of incompressible viscous fluids and the determination of the criterion; *Phil. Trans. Roy. Soc. A* **186** 123–164, https://doi.org/10.1098/rsta.1895.0004.

Ryan J A and Lucich R D 1983 Possible dust devils, vortices on Mars; *J. Geophys. Res. Oceans* **88(C15)** 11,005–11,011, https://doi.org/10.1029/JC088iC15p11005.

Schlichting H, Gersten K, Krause E and Oertel H 1955 *Boundary-layer theory;* Vol. **7** New York: McGraw-hill, Part A.

Sengupta T K, De S and Sarkar S 2003 Vortex induced instability of an incompressible wall-bounded shear layer; *J. Fluid Mech.* **493** 277–286, https://doi.org/10.1017/S0022112003005822.

Sengupta A, Suman V K, Sengupta T K and Bhaumil S 2018 An enstrophy based linear and nonlinear instability theory; *Phys. Fluids* **30** 054106, https://doi.org/10.1063/1.5029560.

Shao Y 2008 *Physics and modeling of wind erosion;* Vol. **37,** Springer Science & Business Media, Chapter 3, pp. 60–75.

Sinclair P C 1966 A quantitative analysis of the dust devil; PhD Dissertation, The University of Arizona, pp. 99–124.

Sinclair P C 1973 The lower structure of dust devils; *J. Atmos. Sci.* **30(8)** 1599–1619, https://doi.org/10.1175/1520-0469(1973)030<1599:TLSODD>2.0.CO;2.

Stanzel C, Pätzold M, Greeley R, Hauber E and Neukum G 2006 Dust devils on Mars observed by the high resolution stereo camera; *Geophys. Res. Lett.* **33(11)**, https://doi.org/10.1029/2006GL025816.

Stull R B 2012 *An introduction to boundary layer meteorology*; Vol. **13**, Springer Science & Business Media, Chapter 1–3.

Sutton J L, Leovy C B and Tillman J E 1978 Diurnal variations of the Martian surface layer meteorological parameters during the first 45 sols at two Viking lander sites; *J. Atmos. Sci.* **35(12)** 2346–2355, https://doi.org/10.1175/1520-0469(1978)035<2346:DVOTMS>2.0.CO;2.

Williamson C H 1996 Vortex dynamics in the cylinder wake; *Ann. Rev. Fluid Mech.* **28(1)** 477–539, https://doi.org/10.1146/annurev.fl.28.010196.002401.

Zheng X 2009 *Mechanics of wind-blown sand movements*; Springer Science & Business Media, Chapter 1–2.

Corresponding editor: Amit Kumar Patra